Thermal conductivity and porosity maps for different materials: A combined case study of granite and sandstone

Sébastien Haffen, Yves Géraud, Michel Rosener, Marc Diraison

Thermalconductivityandporositymapsfordifferentmaterials:A combinedcasestudy ofgraniteandsandstone

SébastienHaffen[a,b,*],YvesGéraud[a],MichelRosener[c],MarcDiraison[d]

[a] GeoRessourceslab.,UMR7359,EcoleNationaleSupérieuredeGéologie,UniversitédeLorraine,CNRS,CREGU,2RueduDoyenMarcelRoubault, Vandœuvre-lès-Nancy,F-54501,France [b] TeranovSAS,2RueduDoyenMarcelRoubault,Vandœuvre-lès-Nancy,F-54501,France [c] 78,84e AvenueEst,Blainville,QcJ7C3T3,Canada [d] InstitutdePhysique duGlobedeStrasbourg(IPGS),UMR7516CNRS-UniversitédeStrasbourg/EOST,5rueRenéDescartes,StrasbourgCedex67084,France

Keywords:Thermalconductivitymap, Porositymap, Heterogeneity, Geothermal

abstract

Thanks to thermal conductivity maps, obtained from Optical Scanning method, and porosity maps, inferred from thermal conductivity maps, we have studied petrophysical heterogeneities commonly present in a granitic and sandstone geothermal reservoir (fault zone and permeable layers, respectively). The maps allowed determination of thermal conductivity and porosity variation to millimeter resolution, at a core scale. They permitted precise quantification and determination of the size of petrophysical heterogeneities (thermal conductivity and porosity) induced by rock variability.

1.Introduction

In the current context of commitment to sustainable and renewable energy, many countries worldwide are developing geothermal energy (Dickson and Fanelli, 2003; Lund et al., 2011; Bertani, 2012). To enhance and ensure the economic and technical viability of the heat exchanger at depth, it appears important to improve the knowledge of thermal and hydraulic properties of the targeted reservoir and their behaviors during the exploitation period (see for example Birsch, 1966; Cermak and Rybach, 1982; Haenel et al., 1988; Clauser and Huenges 1995; Clauser 2006; Hartmann et al., 2008). Indeed, these properties play a major role in the planning of geothermal installation and in geothermal modeling.

Through a geothermal reservoir exchanger, fluid flows occur in the fractures and faults connected network and in different sedimentary levels of high permeability (Haffen et al., 2013; Siffert et al., 2013). These fluids present different types of disequilibrium with respect to the surrounding rocks, as well to temperature and chemical composition. Indeed, interaction processes between fluids and rock, which occur over time in the porous space connected to the main fluid flow zone (mass transfer induced by dissolution and precipitation phenomena or mechanical displacement of clayed particles), can provoke damage to the heat exchanger by modifying its permeability and also affect the surface power plant (Norton and Knapp, 1977; Norton, 1979; Seibt and Kellner, 2003; Ungemach, 2003; Fritz et al., 2010; Civan, 2011; Meier et al., 2014).

Thus, thermal conductivity and porosity maps appear to be two key parameters, since they allow the improvement of the targeted rock characterization, notably from information (quantification and size) about potential rock heterogeneities.

Various experimental techniques allowed the characterization of the thermal conductivity and porosity of rock samples (Zinszner and Pellerin, 2007; Tritt, 2004). We developed a new non destructive method based on Optical Scanning (Popov et al., 1999), to quickly map the thermal conductivity and porosity of samples. We present the acquired 2D thermal conductivity maps and the computed 2D porosity maps.

In this paper, we present results for two kinds of rock: granite and sandstone, which both have specific structures (fractures and sedimentary heterogeneities, respectively). These rocks are of special interest because, for continental Europe, high enthalpy geothermal targets are located in the deep part of the sedimentary basin, its basement and its lower levels, including the bottom of the sedimentary cover, which is generally sandstone (Genter et al., 2003; Bourquin et al., 2011).

2.Geological setting and thermal conductivity/porosity maps elaboration

2.1.Sample description

These selected samples are expected to illustrate two kinds of fluid flow networks in deep geothermal targets. First, a granite sample affected by a fracture zone with quartz infilling at the edge of an open fracture is a kind of structure currently described in granitic geothermal fields (Géraud et al., 2010). Second, a sandstone sample is analyzed, where a sedimentological heterogeneity was induced by grain size variation.

The granite sample (K195-4777) was taken from the EPS1 borehole, part of the deep experimental geothermal site of Soultz sous-Forêts (France) in the Upper Rhine Graben (Genter and Traineau, 1992; Rosener, 2007) (Fig. 1a). The sample is located approximately 2162 m deep, in a granite zone that corresponds to a silicified/cataclased hydrothermal alteration facies (Rosener, 2007). This allows the different compartment typically encountered in fault zones to be studied: the protolith, the damaged zone and the fault core (Caine et al., 1996; Géraud et al., 2010; Faulkner et al., 2010). The sample is divided into three zones (Fig. 1a). Zone 1 corresponds to a damaged zone and is an altered zone composed of massive orange feldspar (orthoclase) associated with altered feldspar, some small secondary quartz and black mica. It has an increase in porosity due to an alteration process induced by hydrothermal fluids. Zone 2 is characterized by a sizable concentration of secondary quartz and hardly any altered feldspar. It corresponds to the protolith. Zone 3 shows a partially sealed localized quartz fault core.

The sandstone sample (EPS1 6 1) also came from the EPS1 borehole (Haffen, 2012) (Fig. 2a), and was extracted at a depth of approximately 1214 m, from the Buntsandstein sandstones formation: "Grès Vosgiens" facies (Vernoux et al., 1995; Bourquin et al., 2006). The petrographic facies corresponds to clayed coating sandstone alternating with clean sandstone (see Haffen, 2012; for details). The sample can be divided into two zones (Fig. 2a): zone 1 is composed mainly of fine to very fine dark brown grained sandstone, and zone 2 is mainly made of medium to fine brown grained sandstone. A small fault is marked by a gap of approximately 5 mm, which is sealed off by extremely thin barite precipitation.

2.2.Measurement techniques: thermal conductivity scanner (TCS)

Optical Scanning measurements performed with a TCS (Popov et al., 1999; Popov et al., 2003) deliver a large set of thermal conductivity values faster than classical laboratory techniques, such as with a divided-bar or a lining source (Sass et al., 1971, 1984). The Optical Scanning apparatus corresponds to a mobile block composed of two temperature sensors on either side of a constant and continuous heat source. These three fixed elements are lined-up on the mobile block, parallel to the mobile displacement axis. The block moves under a rail on which the sample to be measured

had been previously placed. Heat source and temperature sensors move at the same relative speed (TCS mobile block velocity: 4.99 mm s^{-1})

along the scanning surface, which is maintained at a constant distance from both sensors. Thus, measuring the sample temperature before and after its heating is rendered feasible. These data, associated with those of the two standards situated either side of the measured sample and having a thermal conductivity known to be close to that of the sample, allow calculating the absolute thermal conductivity of the sample to become possible. This technique therefore permits the obtainment of a profile of thermal conductivity of the sample along a scan line, with a resolution of 1 mm. The scan line is at a maximum of 500 mm, due to the length of the apparatus, while the relative measurement error is approximately 3% of the measured value (Popov et al., 1999). The room where measurements were carried out was kept at a constant

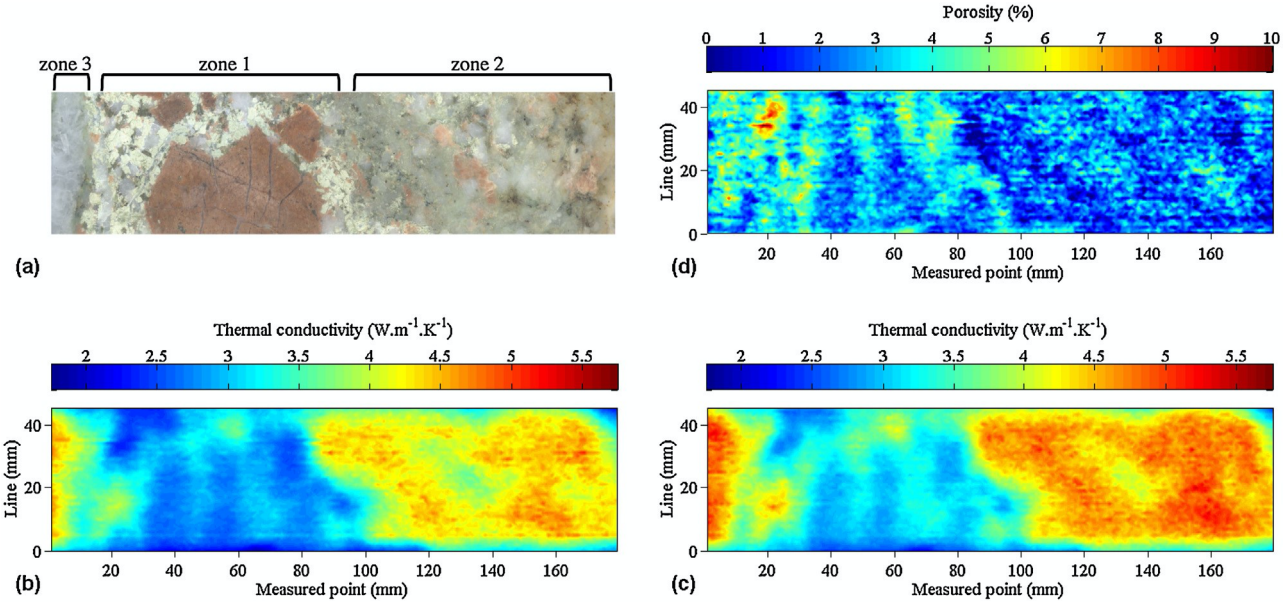

Fig. 1. (a) Analyzed surface of the granite sample; (b) Measured thermal conductivity map of the air saturated granite sample; (c) Measured thermal conductivity map of the water saturated granite sample; (d) Computed porosity map of the granite sample.

temperature (20°C ± 1°C). During the measurements, the increase in sample temperature was limited to 3°C, ranging from 20±1°C to a maximum of 23±1°C. A brief cooling time was systematically imposed between two scan lines to restrict the heating of the sample and of the standards. Thermal conductivity variations induced by the heating of the sample during the measurement were neglected, since at this temperature range the thermal conductivity variation is inferior to the measurement error (Vosteen and Schellschmidt, 2003).

2.3. Thermal conductivity and porosity map

2.3.1. Method

Thermal conductivity in rocks depends mainly on three parameters (e.g. Farouki, 1981; Brigaud and Vasseur 1989; Clauser and Huenges, 1995; Midttomme and Roaldset, 1998): mineralogical composition, porosity and texture. Other parameters can also control the thermal conductivity of rocks as spore fluids properties and structural/textural properties of rocks including rock anisotropy The porosity of a rock can be estimated (Schärli and Rybach, 1982) at constant temperature and pressure, using comparisons between thermal conductivity values obtained for air- and water-saturated samples, while mineralogy and other microstructural parameters are taken as being constant. For each state, the geometric mean model based on mixing laws (Eq. (1), Clauser and Huenges, 1995) is considered, as follows:

$$\ln(\quad) - \ln(\quad)$$

$$= \times 1- \lambda_m \qquad (1)$$

where (Wm^{-1} K^{-1}) is the effective thermal conductivity, (Wm^{-1} K^{-1}) is the thermal conductivity of the fluid (air or water) present in the porosity ((−)), and $_m$ (Wm^{-1} K^{-1}) is the thermal conductivity of the solid matrix.

For a sample, a first set of thermal conductivity measurements under air-saturated conditions and a second set of thermal conductivity measurements under water-saturated conditions are necessary and these lead to the porosity calculation (Eq. (2)) as follows (Pribnow and Sass, 1995; Pribnow et al., 1996; Surma and Geraud, 2003; Haffen, 2012):

$$\ln() - \ln($$

$$= \qquad (2)$$

where $_{sat}$ (Wm^{-1} K^{-1}) is the thermal conductivity of the water-saturated sample, (Wm^{-1} K^{-1}) is the thermal conductivity of the air-saturated sample, $_{wat}$ is the thermal conductivity of water (0.6 Wm^{-1} K^{-1}, Clauser and Huenges, 1995) and is the thermal conductivity of air (0.02 Wm^{-1} K^{-1}, Clauser and Huenges, 1995).

Thus, to calculate porosity, we have considered a simplified case, without needing to build an empirical model (Somerton, 1992). Satisfying results were obtained with the applied mathematical model, based on a mixing law (Pribnow et al., 1996; Hartmann et al., 2005).

This mathematical model (Eq. (2)) was used to determine the mean porosity value from measurements of the thermal conductivity in both dry and wet samples. Here, we use the Optical Scanning method to measure the thermal conductivity. From these measurements and the experimental measurement protocol first proposed by Rosener (2007), we can build a 2D porosity map from 2D thermal conductivity maps. This approach let us observe millimeter scale variations of thermal conductivity and porosity for pluri-decimeter rock samples.

2.3.2. Map construction

Before measurements, surfaces of the samples that were going to be mapped were sawed with a diamond saw and the surfaces were carefully brushed to remove dust. So that all the surfaces have the same albedo and to avoid interference with the measurements they were painted black with spray paint, such that paint-crushing thickness was limited. Then the samples were dried at 60◦C until they reached a constant weight. Several hours before starting the test, the samples were placed in the measurement room, so as to keep them at thermal equilibrium under dry conditions.

The samples were first placed on the TCS rail, at the beginning of the measurements. A profile of thermal conductivity was then determined along a scan line (line000), at each millimeter (point 1, point 2, etc., to the mth point). Later, with great accuracy, the samples were shifted 1 cm perpendicular to the measurement axis and a new profile was created (line010). The measurement sequence has been defined as follows (Fig. 3): line000, line010, line020, line030, etc. line001, line011, line021, line031, etc. line002, line012, line022, line032, etc. line003, line013, line023, line033, etc.

...

until the surfaces were completely scanned. This sequence was developed to limit the heating of the sample, which could

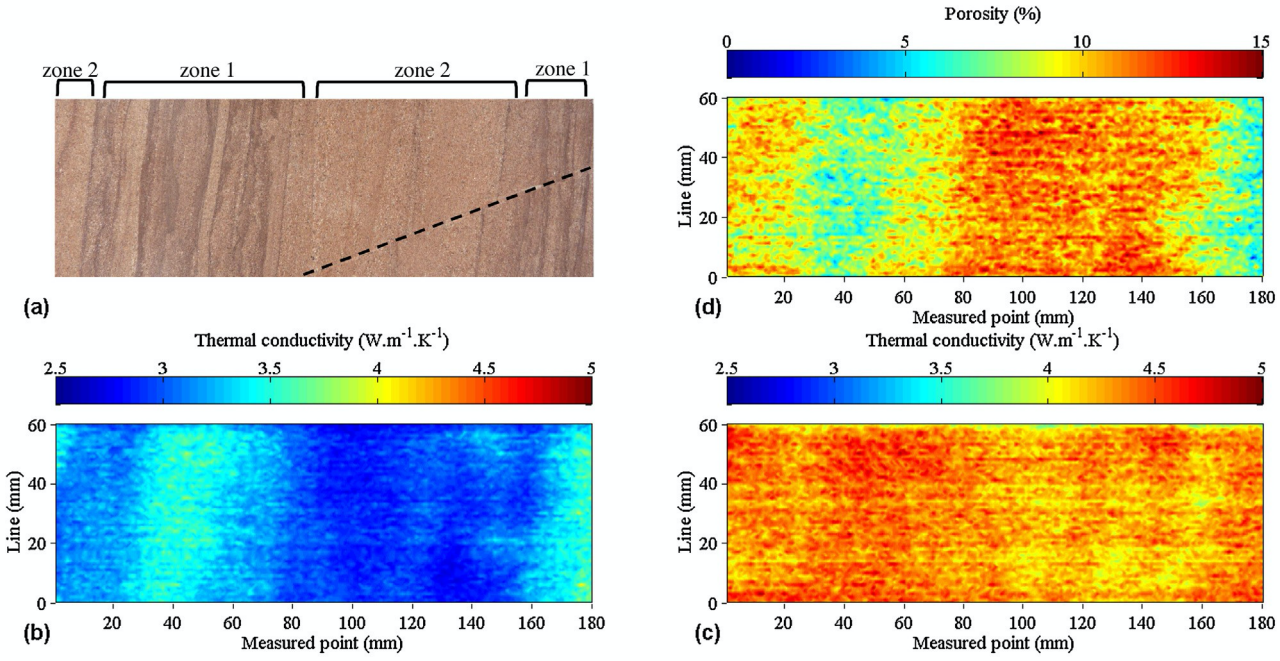

Fig. 2. (a) Analyzed surface of the sandstone sample, black dotted line indicates the sealed fault; (b) Measured thermal conductivity map of the air-saturated sandstone sample; (c) Measured thermal conductivity map of the water-saturated sandstone sample; (d) Computed porosity map of the sandstone sample.

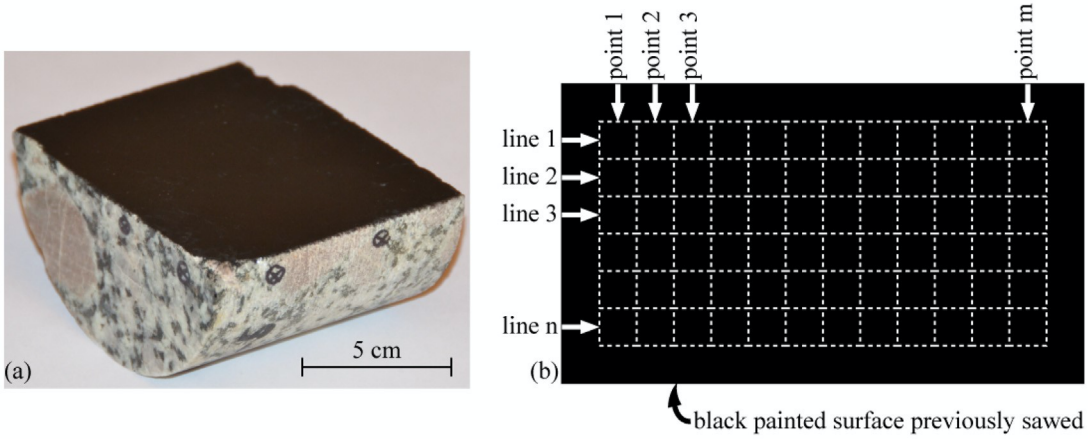

Fig. 3. (a) Photograph of a granite sample prepared for measurement, (b) Schematic representation of the sample's scanned surface, indicating the position of the mth measured point of the nth measured line.

modify the thermal conductivity with an increase in temperature (e.g. Abdulagatova et al., 2009). As a result, each measured point is about 1 mm away from the other measured points surrounding it. These data led to a 2D thermal conductivity map of air-saturated samples (n line × m point/line) with a resolution of 1 mm.

After obtaining the first thermal conductivity map, the samples were water-saturated by submerging them in distilled water inside a sealed vacuum chamber for 48 h. The thermal conductivity maps for water-saturated samples were derived similarly to the previous dry test. The objective was to accurately superpose the two measured surfaces: line XXX (under dry conditions) had to be in strictly the same position as line XXX' (under water-saturated conditions). To limit the evaporation risk, each sample except the measured surfaces was wrapped in plastic film. Weight measurement tests, performed on water-saturated samples before and after thermal conductivity measurements indicated that water loss was lower than 1%.

Thermal conductivity maps could be drawn for each sample, under air- and water-saturated conditions and a porosity map could be computed from these by transforming Eq. (2) in the following way (Eq. (3)):

For all i = 1,...,n and j = 1,...,m

$$\phi_{i,j} = \frac{\ln\left(\lambda_{i,j}\right) - \ln\left(\lambda_{(sat)dry\,i,j}\right)}{\ln\left(\lambda_{wat}\right) - \ln\left(\lambda_{air}\right)} \quad (3)$$

where $\phi_{i,j}$ (−) is the porosity at the mth point of measurement of the nth line, $\lambda_{(sat)i,j}$ (Wm-K-) is the thermal conductivity of the water-saturated sample at the mth point of measurement of the nth line and $\lambda_{(dry)i,j}$ (Wm-K-) the thermal conductivity of the dry sample at the mth point of measurement of the nth line.

Table 1
Statistical data of thermal conductivity and porosity for the two studied samples (std.: standard deviation; m_1: weight of the air saturated sample; m_2: weight of the water saturated sample; m_3: weight of the sample under hydrostatic condition).

Sample	Scanned surface (length×width) (mm)	Thermal conductivity map ($Wm^{-1}K^{-1}$)					Porosity map (%)				Water porosity			
		Saturation	mean	std.	min.	max.	mean	std.	min.	max.	m_1 (g)	m_2 (g)	m_3 (g)	(%)
Granite (K195-4777)	180×50	air	3.49±0.10	0.70	1.84	6.36	2.87±0.14	1.52	0.01	9.85	602.80	609.61	374.67	2.90±0.09
		water	3.81±0.11	0.72	2.04	7.08								
Sandstone (EPS1 6 1)	181×61	air	4.28	3.13	0.13	0.09	0.18	0.23	2.53	3.59	4.93	9.27±0.46	1.98	0.72	16.22	1048.45	1092.44	649.08	9.92±0.30
		water	4.12																

2.3.3. Water saturation test

For each sample, the mean porosity value obtained from thermal conductivity measurements could be compared to the total porosity measured from the water saturation test (Melnyk and Skeet, 1986). This value was obtained from an experimental protocol based on the water saturation of a sample after vacuum degassing. Initially, samples were dried at 60 °C until their weight became constant (m_1 in g) and were later placed in a vacuum chamber for 24 h (after thermal conductivity measurements were performed on dry samples). In the meantime, distilled water was degassed and then used to fill the samples by capillarity. The level of water in the samples was regularly adjusted according to the capillary fringe. Once they were entirely submersed, the vacuum was broken and the samples retained in water for 24 h until they reach a constant weight. Prior to thermal conductivity measurements being carried out on water-saturated samples, the samples were weighed twice: firstly, under water-saturated conditions (m_2 in g) and secondly, under hydrostatic conditions (m_3 in g). Porosity (in %) was calculated as follows (Eq. (4)):

$$= \frac{m_2 - m_1}{m_2 - m_3} \times 100 \quad (4)$$

3. Results

Using TCS, both air-and-water saturated thermal conductivity 2D maps were obtained for the granite and sandstone samples. From these maps, a porosity 2D map was calculated. Histograms of thermal conductivity and porosity distribution were plotted from the previous maps, to define a relationship between porosity and mineralogy.

For the two samples analyzed, statistical data of thermal conductivity and porosity are given in Table 1. Thermal conductivity and porosity maps for the granite and sandstone samples are presented in Figs. 1 and 2, respectively. Histograms of thermal conductivity and porosity distribution for the granite and sandstone samples are given in Figs. 4 and 5 respectively. The distribution of thermal conductivity depending on porosity is also given in Figs. 4 and 5, respectively, for the granite and sandstone samples.

3.1. Granite sample

The three structural zones described in Fig. 1a were identified on thermal conductivity maps of the sample under both air and water-saturated conditions (Fig. 1b,c). The thermal conductivity values for zone 1 ranged from about 1.80–3.60 $Wm^{-1}K^{-1}$ for the air-saturated sample and from about 2.00–4.25 $Wm^{-1}K^{-1}$ for the water-saturated sample. For zone 2, the thermal conductivity values ranged from about 3.60–5.00 $Wm^{-1}K^{-1}$ and from 3.75 to 5.25 $Wm^{-1}K^{-1}$ for the air- and water-saturated samples, respectively. The thermal conductivity values for zone 3 ranged from about 3.60–4.90 $Wm^{-1}K^{-1}$ and from about 3.75–5.50 $Wm^{-1}K^{-1}$ for the same samples. The porosity map (Fig. 1d) indicates that the values of zone 1 ranged from zero to ten%, those of zone 2 ranged between zero and five% and the porosity values of zone 3 ranged from zero up to about eight%. Thus, the quartz cementation in the matrix (zone 2) tended to increase the local thermal conductivity and to decrease the local porosity, while conversely feldspar alteration decreased the local thermal conductivity and increased the local porosity (zone 1).

Histograms of thermal conductivity distribution, under both air and water-saturated conditions for the granite sample (Fig. 4a,b) presented the same bimodal global trend, with two well-marked peaks of measured thermal conductivity values. In the air-saturated case (Fig. 4a), peaks were centered on 2.90 and 4.17 $Wm^{-1}K^{-1}$, with a gap of about 1.27 $Wm^{-1}K^{-1}$. In the water-saturated case (Fig. 4b), peaks were centered on 3.25 and 4.50 $Wm^{-1}K^{-1}$, with a gap of about 1.25 $Wm^{-1}K^{-1}$. A comparison between thermal conductivity histograms and maps suggested that for both air and water-saturated cases, the lower value peaks corresponded to zone 1, composed mainly of massive feldspar associated with altered feldspar and some small secondary quartz (theoretical thermal conductivity values: Quartz=7.8 $Wm^{-1}K^{-1}$, Feldspar-

(theoretical thermal conductivity values: Biotite=2.3Wm-1 K-1, air=0.02Wm-1 K-1, water=0.6Wm-1 K-1, Clauser and Huenges, 1995; Fjeldskaar et al., 2009). At the same time, peaks of the higher values of thermal conductivity, for both air- and water-saturated cases, corresponded to a mixture of zone 2 and zone 3, both mainly composed of quartz. The gap between the theoretical and measured thermal conductivity in these two zones can be explained by the porosity and the presence of small amounts of feldspar and mica, which have lower thermal conductivity values than quartz and can modify the contact between grains

2009). The histogram of porosity distribution (Fig. 4c) shows a unimodal global trend (Gaussian shape) with a maximum of calculated points for a porosity value of about 2.60%. This behavior can be explained by constant gaps between peaks of thermal conductivity, whatever the saturation condition. The saturation of the sample by water provoked a linear increase in thermal conductivity in all three structural zones of the sample. The distribution of thermal conductivity (air-saturated condition) depending on the porosity (Fig. 4d)

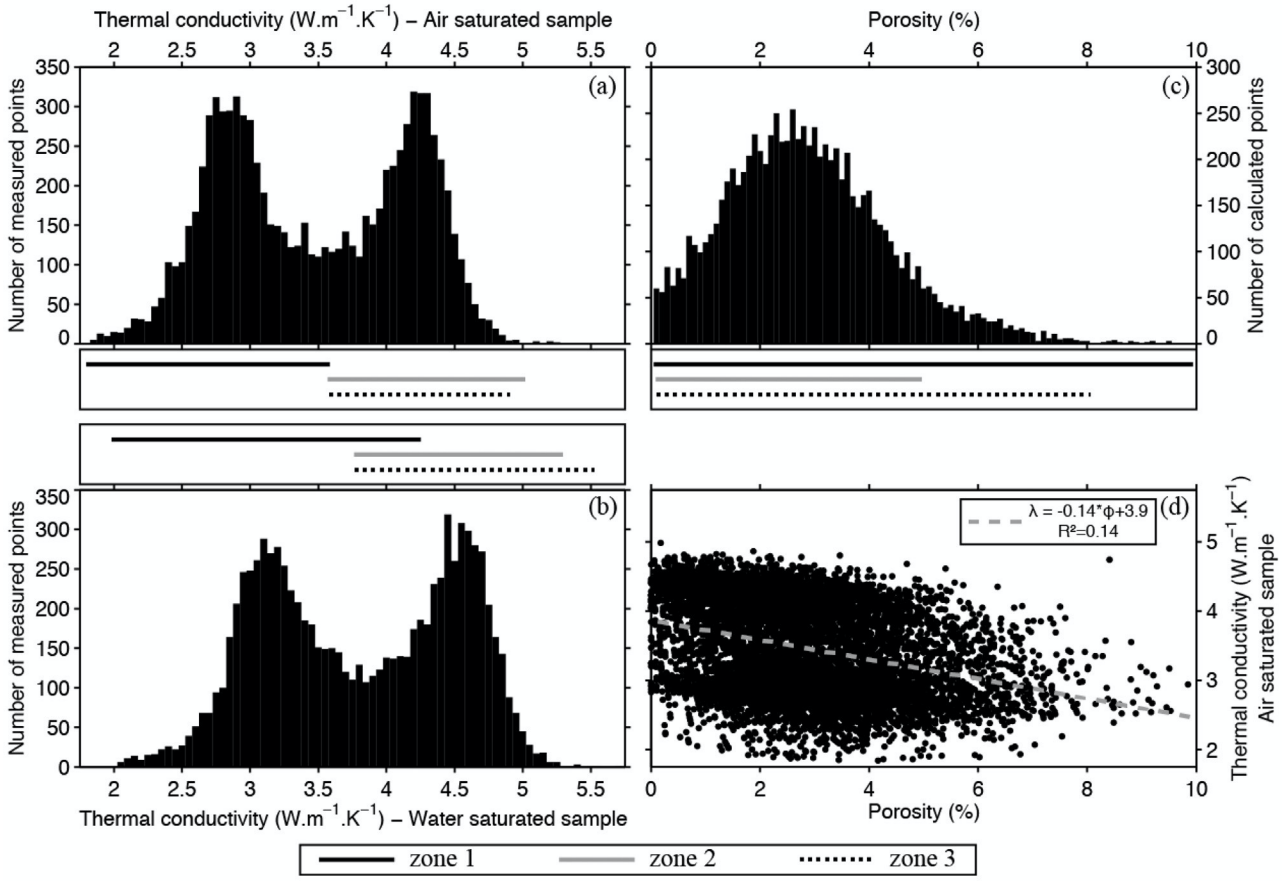

Fig. 4. Granite sample: (a), (b), distribution of measured thermal conductivity values, in the air and water saturated sample respectively (column width: 0.05Wm-1 K-1); (c) distribution of the calculated porosity values (column width: 0.1%); (d) relationship between calculated porosity values and measured thermal conductivity values of the air saturated sample.

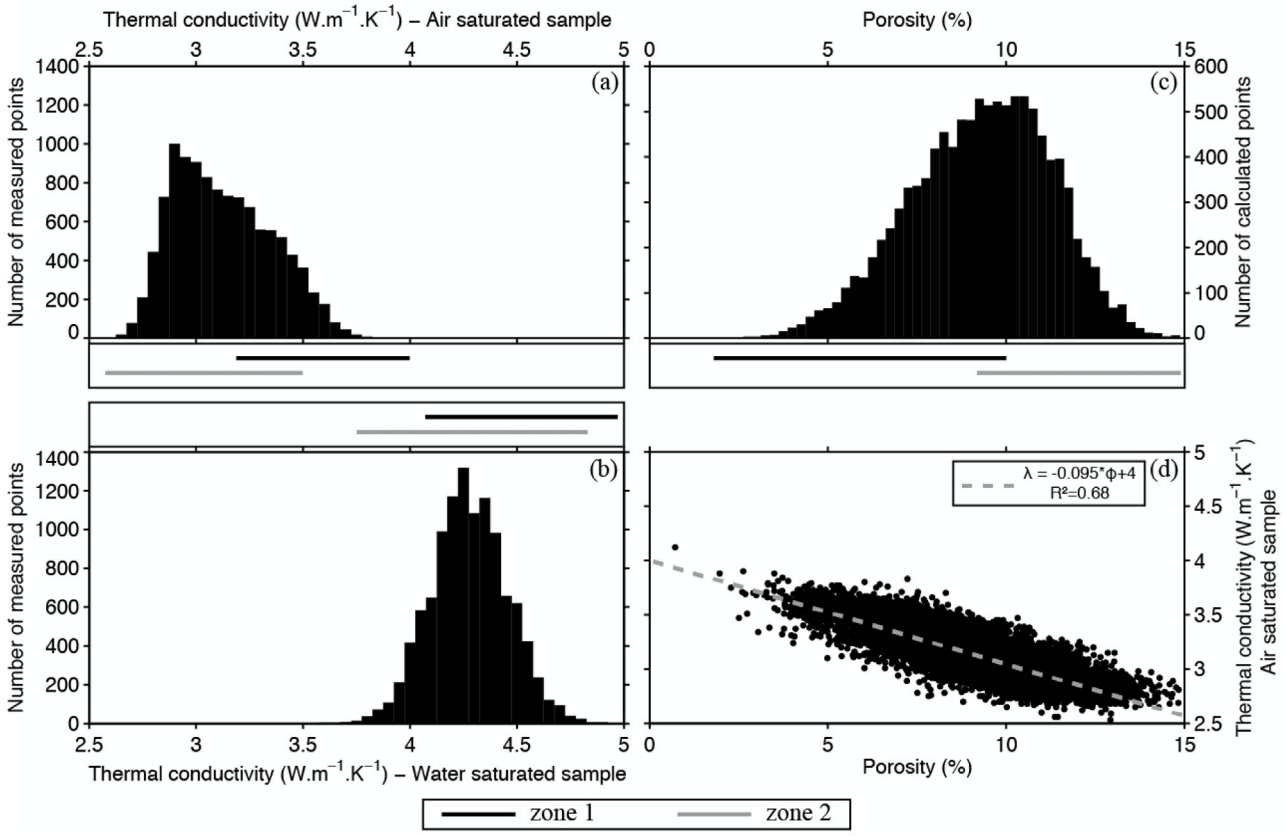

Fig. 5. Sandstone sample: (a), (b), distribution of measured thermal conductivity values, in the air and water saturated sample respectively (column width: 0.05Wm^{-1} K^{-1});

(c) distribution of the calculated porosity values (column width: 0.25%); (d) relationship between calculated porosity values and measured thermal conductivity values of the air saturated sample.

indicated a global but not well-marked decrease of thermal conductivity, while the porosity increased (simple linear regression: $\lambda = -0.14^{*}\Phi+3.9$). The two peaks observed in Fig. 4a and b were also denoted by a poorly-marked decrease of thermal conductivity and a porosity increase. Thus, mineralogical distribution throughout the sample plays a major role in the thermal conductivity, whereas the porosity is less sensitive to mineralogical distribution.

The mean porosity (Table 1) calculated from thermal conductivity maps is 2.87 ± 0.14%, close to the water porosity value of 2.90±0.09%.

3.2. Sandstone sample

The two zones described in Fig. 2a could be identified on the thermal conductivity map of the dry sample (Fig. 2b). Zone 1 indicated thermal conductivity values ranging between 3.20 and 4.00Wm^{-1} K^{-1} whereas zone 2 showed thermal conductivity values ranging from 2.60 to 3.50Wm^{-1} K^{-1}. The thermal conductivity map of the water-saturated sample (Fig. 2c) appeared more homogeneous than that of the dry sample. In zone 1, the thermal conductivity values ranged between 4.10 and 5.00Wm^{-1} K^{-1} whereas in zone 2 values were comprised between 3.75 and 4.80Wm^{-1} K^{-1}. The porosity map (Fig. 2d) displayed two main zones located at the level of the main structures (Fig. 2a). Zone 1 had porosity values ranging between two and ten% whereas the porosity values were comprised between nine and fifteen% for zone 2. However, the small fault does not appear on thermal conductivity and porosity maps. Thus, the decrease in the grain size (from zone 2 to zone 1) resulted in an increase in the thermal conductivity associated with a decrease in the local porosity.

For the sandstone sample, histograms of thermal conductivity distribution under both air- and water-saturated conditions (Fig. 5a, b) presented the same unimodal global trend, with one peak of measured thermal conductivity values. In the air-saturated case (Fig. 5a), the peak showed a maximum at 2.9Wm^{-1} K^{-1}, while in the water-saturated case (Fig. 5b), the equivalent was about 4.25Wm^{-1} K^{-1}. The comparison between thermal conductivity histograms and maps in air-saturation conditions, suggested that the lower values of thermal conductivity in the peaks corresponded to zone 2, composed mainly of medium grains, whereas the higher values of thermal conductivity corresponded to zone 1, composed mainly of fine grains. The same trend was less-marked under water-saturation conditions. The histogram of porosity distribution (Fig. 5c) showed a unimodal global trend, with a maximum of calculated points for a porosity value of about 10.40%. The lower values in the peak of porosity corresponded to zone 1, whereas the higher values corresponded to zone 2. The global high values of porosity in the sample and the presence of a clayed coating could explain the low thermal conductivity measured under dry conditions (theoretical thermal conductivity values for Illite grains=1.9Wm^{-1} K^{-1},

Clauser and Huenges, 1995; Fjeldskaar et al., 2009) and the increase of thermal conductivity values under water-saturated conditions (The gap between the maximum thermal conductivity under air or water-saturated conditions is about 1.35 $Wm^{-1} K^{-1}$). The distribution of thermal conductivity (air-saturated condition) depending on the porosity (Fig. 5d) indicated a global decrease of thermal conductivity with the porosity increase (simple linear regression: $= -0.095 * \Phi + 4$). Thus, the grain size variation in laminae, associated with mineralogical small variations, led to a modification in the thermal conductivity and porosity distribution at the millimeter scale. These variations seem to be continuous at the core scale.

The mean porosity (Table 1) deduced from thermal conductivity maps is 9.27± 0.46%, close to the porosity value obtained from mass weight during a water saturation test: 9.92±0.30%.

4. Discussion

- Map construction

The thermal conductivity and porosity maps were obtained from successive measurements, through the scanning of a sample saturated with both air and water. The TCS allows measurements of the thermal conductivity profile to be made, at a density of one point per millimeter. From a profile carried out at each millimeter, the calculation of a porosity value for each millimeter square of a sample surface is made possible. For each sample analyzed, relatively similar porosity values have been determined from both thermal conductivity and water saturation tests (Table 1). Nevertheless, variations are observed and these can be explained by the following three parameters: the first is the result of the difference between the volumes investigated by the two methods. The entire volume of a sample is analyzed during water porosity measurements, whereas a more limited volume under the scanning surface is analyzed by the thermal conductivity measurements (Popov, 1997), where the volume investigated is 2.5 cm maximum thick. The second involves the modification of the contact resistance between the different components of a rock sample resulting from water saturation and could thus alter the thermal conductivity characteristics (e.g. Farouki, 1981). The third is induced by a relatively significant gap between the thermal conductivity of the standards and that of the sample: a larger gap would trigger a more extensive mistake of the thermal conductivity value. Indeed, for the granite sample, thermal conductivity variations between the air and water- saturated conditions are low and induce no change in standards when the experimental values remain close to standard ones. For the sandstone sample, the relative high porosity of the material implies a change in standards between the air- and water saturated conditions. Standards used for the air-saturated sample measurements have a relatively low thermal conductivity value for the water-saturated sample measurements. This gap induces the underestimation of the porosity from the thermal conductivity measurements.

- Information about samples

The granite and sandstone samples are both mainly composed of quartz and feldspar. However, the thermal conductivity maps and histograms of thermal conductivity distribution are different, with a bimodal distribution for the granite and a unimodal distribution for the sandstone. These feature can be explained by the well-marked difference of thermal conductivity between quartz and feldspar, associated with the size of the grains in the samples: coarse in the granite and fine to medium in the sandstone, and by the fact that the TCS cannot individualize fine grain properties (lower to a few-millimeters in scale).

In granite and sandstone samples, the porosity distribution is quite heterogeneous, i.e. there are variations in the localization of the most (and the lesser) porous zones, although the distribution of the porosity is unimodal in both cases. In the granite sample, the porosity is controlled by structural heterogeneities: the porosity is mainly located near the fault along grain borders in an altered zone where hydrothermal fluids have partially dissolved the grains. In the sandstone sample, the porosity is controlled by sedimentological heterogeneities: the porosity appears according to a layered organization. Inside each layer, the porosity is quite homogeneous. The porosity varies in function of the facies distribution and is controlled by grains size inside each band. Thus, porosity variations, inside both samples, are not extremely 'cut', there is progressive transition between the most and the less porous zones, at the scale of the sample.

In the granite sample, constant gaps between peaks of thermal conductivity distribution, whatever the saturation condition, were observed. The saturation of the sample by water provokes a linear increase in the thermal conductivity in the structural zones of the sample. Thus, the percentage increase in thermal conductivity induced by water is higher for the peak corresponding to the lower thermal conductivity, i.e. the feldspar-rich zone, than the one corresponding to the higher thermal conductivity, i.e. the quartz-rich zone.

The thermal conductivity and porosity maps present values that are in agreement with other classical measurements performed on equivalent materials, using the same or other techniques (Vernoux et al., 1995; Sizun, 1995; Surma and Géraud, 2003; Haffen, 2012). Nevertheless, the mapping of these physical properties brings more information, notably concerning the location of the most, or less, porous and conductive zones in samples. These zones can be linked to structural and petrographic features and so lead to the improvement of the knowledge of fluid and heat exchanges in reservoirs.

5. Conclusion

From thermal conductivity and porosity maps, we have put forward the impact of petrophysical heterogeneities commonly present in a granite and sandstone geothermal reservoirs, i.e. fault zone and permeable layers respectively. The maps allow the study of thermal conductivity and porosity variation, at millimetric resolution and at core scale. From two scans of a sample surface, in air-saturated conditions on the one hand, and in water-saturated conditions on the other hand, porosity maps can be established. These allow precise quantification and determination of the size of thermal conductivity and porosity heterogeneities induced by rock heterogeneities.

Acknowledgments

The authors would like to thank EEIG Heat Mining and A. Genter (ES Geothermie), the scientific coordinator, for allowing access to the cores of the EPS1 borehole.

References

Abdulagatova, Z., Abdulagatov, I.M., Emirov, V.N., 2009. Effect of temperature and pressure on the thermal conductivity of sandstone. Int. J. Rock Mech. Min. Sci. 46, 1055–1071.

Bertani, R., 2012. Geothermal power generation in the world 2005–2010 update report. Geothermics 41, 1–29.

Birsch, F., 1966. Thermal conductivity and diffusivity. In: Clark, S.P. (Ed.), Handbook of Physical Constants, Rev. Eds., Memoir, Vol. 97. Geological Society of America, pp. 97–173.

Bourquin, S., Péron, S., Durant, M., 2006. Lower Triassic sequence stratigraphy of the western part of the German Basin (west of Black Forest): Fluvial system evolution through time and space. Sediment. Geol. 186, 187–211.

Bourquin, S., Bercovici, A., Lopez-Gomez, J., Diez, J.B., Broutin, J., Ronchi, A., Durant, M., Arché, A., Linol, A., Amour, F., 2011. The Permian-Triassic transition and the onset of Mesozoic sedimentation at the northwestern peri-Tethyan domaine scale: palegeographic map and geodynamic implication. Paloegeography, Paleoclimatology, Paleoecology 299, 265–280.

Brigaud, F., Vasseur, G., 1989. Mineralogical, porosity and fluid control on the thermal conductivity of sedimentary rocks. Geophys. J. 98, 525–542.

Caine, J.S., Evans, J.P., Forster, C.B., 1996. Fault zone architecture and permeability structure. Geology 24, 1025–1028.

Cermak, V., Rybach, L., 1982. Thermal Conductivity and Specific Heat of Minerals and Rocks In Landolt-Börnstein, New Series, Group V (1a): Geophysics. Springer, pp. 305–343.

Civan, F., 2011. Porous Media Transport Phenomena. John Wiley & Sons, USA (400p.).

Clauser, C., Huenges, E., 1995. Thermal conductivity of rock and minerals. In: Ahrens, T.J. (Ed.), Rock Physics and Phase Relation - a Handbook of Physical Constants, Vol. 3. AGU reference shelf, pp. 105–126.

Clauser, C., 2006. Geothermal energy. In: Heinloth, K. (Ed.), Landolt-Börnstein, Group VIII: Advanced Material and Technologies, Vol. 3: Energy Technology, Subvol. C: Renewable Energy. Springer, pp. 493–604.

Dickson, M.H., Fanelli, M., 2003. Geothermal Energy: Utilization and Technology (ISBN 92-3-103915-6. 221p.).

Farouki, O., 1981. Thermal Properties of Soils, CRREL Monograph 81-1. US Army Cold Region Research and Engineering, Hanover New Hampshire, USA (151p.).

Faulkner, D.R., Jackson, C.A.L., Lunn, R.J., Schlische, R.W., Shipton, Z.K., Wibberley, C.A.J., Withjack, M.O., 2010. A review of recent developments concerning the structure, mechanics and fluid flow properties of fault zones. J. Struct. Geol. 32, 1557–1575.

Fjeldskaar, W., Christie, O.H.J., Midttomme, K., Virnovsky, G., Jensen, N.B., Lohne, A., Eide, G.I., Balling, N., 2009. On the determination of thermal conductivity of sedimentary rocks and the significance for basin temperature history. Pet. Geosci. 15, 367–380.

Fritz, B., Jacquot, E., Jacquemont, B., Baldeyrou-Bailly, A., Rosener, M., Vidal, O., 2010. Geochemical modelling of fluid–rock interactions in the context of the Soultz-sous-Forêts geothermal system. C.R. Geosci. 342(7), 653–667.

Géraud, Y., Rosener, M., Surma, F., Place, J., LeGarzic, E., Diraison, M., 2010. Physical properties of fault zones within a granite body: example of the Soultz-sous-Forêts geothermal site. C.R. Geosci. 342, 566–574.

Genter, A., Traineau, H., 1992. Borehole EPS1: Alsace France: preliminary geological results from granite core analysis for Hot Dry Rock research. Sci. Drill. 3, 205–214.

Genter, A., Guillou-Frottier, L., Feybasse, J.L., Nicol, N., Dezayes, C., Schwartz, S., 2003. Typology of potential hot fractured rock ressouces in europe. Geothermics 32, 701–710.

Haenel, R., Rybach, L., Stegena, L., 1988. Handbook of Terrestrial Heat-Flow Density Determination. Kluwer Academic Publishers, Dordrecht.

Haffen, S., Géraud, Y., Diraison, M., Dezayes, C., 2013. Fluid-flow zones in a geothermal sandstone reservoir: localization from thermal conductivity and temperature logs, borehole EPS1 (Soultz-sous-Forêts, France) and 3D models. In: Proceedings, Thirty-Eighth Workshop on Geothermal Reservoir Engineering, Stanford University, Stanford, California, February 11–13, 2013 (SGP-TR-198).

Haffen, S., 2012. Caractéristiques géothermiques Du réservoir Gréseux Du Buntsandstein d'Alsace. Thesis. Institut de Physique du Globe de Strasbourg, Université de Strasbourg, Strasbourg, France (391p. In French).

Hartmann, A., Rath, V., Clauser, C., 2005. Thermal conductivity from core and well log data. Int. J. Rock Mech. Min. Sci. 42, 1042–1055.

Hartmann, A., Pechnig, R., Clauser, C., 2008. Petrophysical analysis of regional-scale thermal properties for improved simulations of geothermal installations and basin-scale heat and fluid flow. International Journal of Earth Science GR 97, 421–433.

Lund, W.J., Freeston, D.H., Boyd, T.L., 2011. Direct utilization of geothermal energy 2010 worldwide review. Geothermics 40, 159–180.

Meier, D.B., Gunnlaugsson, E., Gunnarsson, I., Jamtveit, B., Peacock, C.L., Benning, L.G., 2014. Microstructural and chemical variation in silica-rich precipitates at the Hellisheioi geothermal power plant. Mineral. Mag. 78(6), 1381–1389.

Melnyk, T.W., Skeet, A.M.M., 1986. An improved technique for the determination of rock porosity. Canadian Journal of Earth Science 23, 1068–1074.

Midttomme, K., Roaldset, E., 1998. The effect of grain size on thermal conductivity of quartz sands and silts. Pet. Geosci. 4, 165–172.

Norton, D., Knapp, R., 1977. Transport phenomena in hydrothermal systems: the nature of porosity. Am. J. Sci. 277, 913–917.

Norton, D., 1979. Transport phenomena in hydrothermal systems: the redistribution of chemical components around cooling plutons. Bull. Mineral. 102, 471–486.

Popov, Y.A., Pribnow, D.F.C., Sass, J.H., Williams, C.F., Burkhardt, H., 1999. Characterization of rock thermal conductivity by high-resolution optical scanning. Geothermics 28, 253–276.

Popov, Y.A., Pohl, J., Romushkevich, R., Tertychnyi, V., Soffel, H.C., 2003. Geothermal characteristics of the Ries impact structure. Geophys. J. Int. 154(2), 355–378.

Popov, Y.A., 1997. Optical scanning technology for nondestructive contactless measurements of thermal conductivity and diffusivity of solid matters. Brussels, Belgium In: Experimental Heat Transfer, Fluid Mechanics and Thermodynamics Proceedings of the 4th World Conference, 1, pp. 109–117.

Pribnow, D.F.C., Sass, J.H., 1995. Determination of thermal conductivity for deep boreholes. J. Geophys. Res. 100, 9981–9994.

Pribnow, D.F.C., Williams, C.F., Sass, J.H., Keating, R., 1996. Thermal conductivity of water-saturated rocks from the KTB pilot hole at temperature of 25–300 °C. Geophysical Research Letter 23, 391–394.

Rosener, M., 2007. Etude pétrophysique Et Modélisation Des Effets Des Transferts Thermiques Entre Roche Et Fluide Dans Le Contexte géothermique De Soultz-sous-Forêts. Thesis. Institut de Physique du Globe de Strasbourg, Université Louis Pasteur, Strasbourg, France (207p. In French).

Sass, J.H., Lachenbruch, A.H., Munroe, R.J., 1971. Thermal conductivity of rocks from measurements on fragments and its application to heat-flow determination. J. Geophys. Res. 76, 3391–3401.

Sass, J.H., Stone, C., Munroe, R.J., 1984. Thermal conductivity determinations on solid rock – a comparison between steady state divided bar apparatus and a commercial transient line-source device. J. Volcanol. Geotherm. Res. 20, 145–153.

Schärli, U., Rybach, L., 1982. On the thermal conductivity of low-porosity crystalline rocks. Tectonophysics 103, 307–313.

Seibt, P., Kellner, T., 2003. Practical experience in the reinjection of cooled thermal water back into sandstone reservoirs. Geothermics 32, 733–741.

Siffert, D., Haffen, S., Garcia, M.H., Géraud, Y., 2013. Phenomenological study of temperature gradient anomalies in the Buntsandstein formation, above the Soultz geothermal reservoir, using TOUGH2 simulations. In: Proceedings, Thirty-Eighth Workshop on Geothermal Reservoir Engineering, Stanford University, Stanford, California, February 11–13, 2013 (SGP-TR-198).

Sizun, J.P., 1995. Modification Des Structures De Porosité De Grès Lors De Transformations pétrographiques Dans La Diagenèse Etl'hydrothermalisme Thèse. Institut de Géologie. Strasbourg, Université Louis Pasteur, Strasbourg, France (297p. In French).

Somerton, W.H., 1992. Thermal Properties and Temperature–related Behaviour of Rock/fluid System. Elsevier Science Publishing Company, New York (257p.).

Surma, F., Geraud, Y., 2003. Porosity and thermal conductivity of the soultz-sous-Forêts granite. Pure Appl. Geophys. 160, 1125–1136.

Tritt, T.M., 2004. Thermal conductivity, theory, properties and application. In: Tritt, Terry (Ed.), Physics of Solids and Liquids), Includes Bibliographical References and Index. Kluwer Academic/Plenum Publishers, New York (290p.).

Ungemach, P., 2003. Reinjection of cooled geothermal brines into sandstone reservoirs. Geothermics 32, 743–761.

Vernoux, J.F., Genter, A., Razin, P., Vinchon, C., 1995. Geological and petrophysical parameters of a deep fractured sandstone formation as applied to geothermal exploitation. In: Rapport BRGM R38622. EPS-1 borehole, Soultz-sous-Forêts, France (70p., 24 fig., 5 tabl., 3 append).

Vosteen, H.D., Schellschmidt, R., 2003. Influence of temperature on thermal conductivity, thermal capacity and thermal diffusivity of different types of rock. Phys. Chem. Earth 28, 499–509.

Zinszner, B., Pellerin, F.M., 2007. A Geoscientist's Guide to Petrophysics. IFP Publication, Edition TECHNIP, Paris, France, pp. 384p.